Topological phases via engineered orbital hybridization in noncentrosymmetric optical lattices

Bo Liu, Xiaopeng Li, and W. Vincent Liu

Topological phases via engineered orbital hybridization in noncentrosymmetric optical lattices

Bo Liu,[1,2] Xiaopeng Li,[3] and W. Vincent Liu[1,2,*]

[1]*Department of Physics and Astronomy, University of Pittsburgh, Pittsburgh, PA 15260, USA*
[2]*Wilczek Quantum Center, Zhejiang University of Technology, Hangzhou 310023, China*
[3]*Condensed Matter Theory Center and Joint Quantum Institute,*
University of Maryland, College Park, MD 20742, USA

We propose a symmetry-based method of using noncentrosymmetric optical lattices to systematically control topological non-trivial orbital hybridization. A crucial difference from the previous studies is the role of inversion symmetry breaking, which is applied to induce an exotic orbital-changing hopping perpendicular to the direction without inversion symmetry and opens a band gap, instead of reducing the codimension and producing gapless points. The orbital mixing here is reminiscent of the spin-orbit physics based on hyperfine states but differs in symmetry and origin. This non-trivial orbital hybridization produces a topological band structure. Attractively interacting fermionic atoms loaded in such a lattice are found to show an orbital topological Fulde-Ferrell superfluid state in the presence of onsite rotation. This state supports Majorana fermions on its edges. Our mechanism should pave an alternative way to achieve orbital topological phases in optical lattices of non-standard geometry.

I. INTRODUCTION

Symmetry plays an important role in solid state materials and influences many of their properties in a profound way. Recently, the noncentrosymmetric materials, i.e., crystal structure lacking a center of inversion, have attracted considerable theoretical and experimental attention in various fields of condensed matter physics [1]. In contrast to the centrosymmetric case, the absence of inversion symmetry leads to very rich physical phenomena, such as skyrmion states [2–4], novel superconducting phases [5–8], as well as magnetoelectric effect [9, 10]. In parallel to the developments in solid state physics, optical lattices with highly tunable geometry in the recent ultracold atom experiments [11] provide new opportunities to study noncentrosymmetric materials. For example, in 2D noncentrosymmetric optical lattices with Rashba spin-orbit coupling, the possible topological superconducting phases have been discussed [12].

Recent experimental progress in manipulating higher orbital bands in optical lattices [13–17] provides unprecedented opportunities to investigate quantum many-body phases with orbital degrees of freedom. Studying higher orbital physics in optical lattices is attracting considerable interests due to their unique and intrinsic spatial nature [18]. An idea of using orbital hybridization to emulate spin-orbit physics, or artificial gauge fields in general, has emerged in recent theoretical studies [19–23], where various interesting many-body states have been proposed. In the context of periodically driven systems, orbital hybridization is shown to be controllable by lattice shaking [24–26]. However how to systematically control the orbital hybridization in static optical lattices remains unclear and stands as an obstacle to explore the rich phenomena in orbital hybridized many-body ground states.

In this work, we propose a static noncentrosymmetric optical lattice, where the orbital hybridization is systematically controllable by manipulating symmetry breaking. We find topological bands arise from the interplay between higher orbitals and inversion symmetry breaking, yet without requiring Raman-induced spin-orbit coupling nor other artificial gauge field [27, 28]. Furthermore when considering attractive fermionic atoms, say ^{6}Li [29–32] loaded into such a noncentrosymmetric optical lattice, we find an orbital hybridized topological Fulde-Ferrell superfluid state (tFF) in the presence of local orbital angular momentum induced by onsite rotation [33]. The mechanism of realization of this tFF superfluid state is crucially different in symmetry (to be illustrated below) compared to the previous studies based on hyperfine states [34–44]. Moreover, our symmetry-based method of controlling orbital hybridization is in principle applicable to other optical lattice setups as well [19–23, 45, 46], which could lead to more interesting noncentrosymmetric many-body phases worth future exploring.

II. EFFECTIVE MODEL

Let us consider a noncentrosymmetric optical lattice with the potential

$$
\begin{aligned}
V(x, y) &= -V_X \cos^2(k_{Lx}x) - V_Y \cos^2(k_{Ly}y) \\
&+ V_{\bar{Y}} \cos^2(3k_{Ly}y + \theta/2),
\end{aligned}
\tag{1}
$$

where V_X, V_Y, $V_{\bar{Y}}$ are the depth of optical lattices, k_{Lx}, k_{Ly} are the wavevectors of laser fields and the corresponding lattice constants are $a_x = \pi/k_{Lx}$, $a_y = \pi/k_{Ly}$ along the x and y directions, respectively. By the techniques of designing the geometry of optical lattices developed in the recent experimental advances [11], the configuration of optical lattices considered here can be formed through three retro-reflected laser beams as shown in Fig. 1(a). The interference of two perpendicular beams X and Y gives rise to a 2D square lattice. The third beam $\bar{Y}$ creates an additional standing wave pattern which breaks the inversion symmetry along the y direction, for example, as shown in Fig. 1(b).
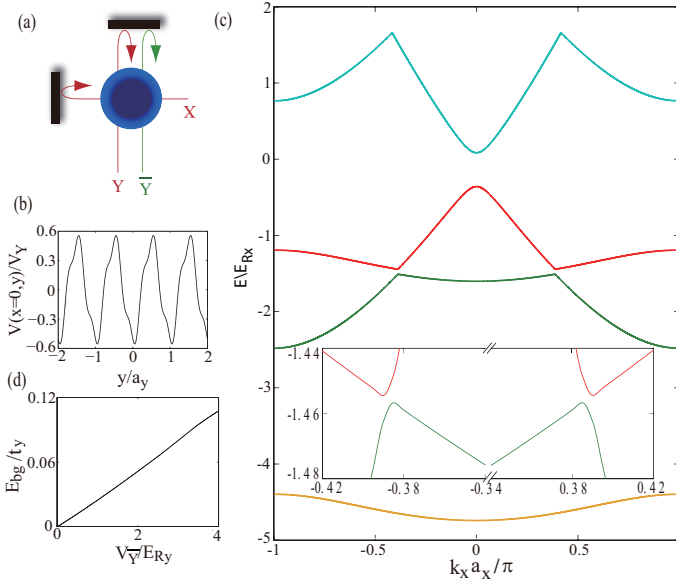
FIG. 1: (a) Three retro-reflected laser beams create the lattice potential in Eq. (1). X and Y interfere and produce a 2D square lattice, while $\bar{Y}$ creates an independent standing wave. (b) Lattice potential along the y direction (dropping a constant) shows the inversion symmetry breaking. (c) The single-particle energy spectrum along k_x axis in the unit of E_{Rx} for the lowest four bands through plane wave expansion calculation. The inset shows the band gap originated from the hybridization between the second and third bands. (d) The hybridization gap as a function of $V_{\bar{Y}}$. In (b), the lattice parameters are chosen as $V_X/E_{Rx} = 4$, $V_Y/E_{Ry} = 40$, $V_{\bar{Y}}/E_{Ry} = 8$ and $\theta = \pi/2$, where the recoil energy is $E_{Rx} = \hbar^2 k_{Lx}^2/2m$ and $E_{Ry} = \hbar^2 k_{Ly}^2/2m$. In (c) and (d), the parameters are chosen as $V_{\bar{Y}}/E_{Ry} = 6$, $\theta = \pi/5$ and $V_X/E_{Rx} = 7$, $\theta = \pi/20$ respectively and other parameters are the same as in (b).

This noncentrosymmetric geometry plays a crucial role in producing the non-trivial Bloch bands in our model, to be illustrated below. Here we consider dynamically anisotropic geometry of the lattice potential by using a larger lattice depth in the y direction, i.e., $V_Y \gg V_X$, while holding the condition $V_X k_{Lx}^2 = V_Y k_{Ly}^2$. As a result, the local rotational symmetry of each site in the xy plane is preserved [45] and the lattice constants simultaneously satisfy $a_y > a_x$. Since the system has relatively stronger potential and larger spacing in the y direction, the tunnelings in the y direction are much weaker than that along the x direction. The band structure of such a lattice system is solved numerically through plane wave expansion. We find that the second and third bands cross in the absence of $V_{\bar{Y}}$. When $\theta \neq \pi$ ($\theta \subset (0, 2\pi)$) and $V_{\bar{Y}} \neq 0$, we see the gap reopening due to inversion symmetry breaking (e.g., Fig. 1(c)). This hybridized gap increases linearly with enlarging $V_{\bar{Y}}$ when $V_{\bar{Y}} \ll V_Y$ as shown in Fig. 1(d). Here we assume the coupling strength between different bands induced by $V_{\bar{Y}}$ is much smaller than the band gap. Therefore, we find that the orbital hybridization only occurs between the second and third bands. The band mixing can thus be turned on and off by controlling the symmetry of the lattice geometry.
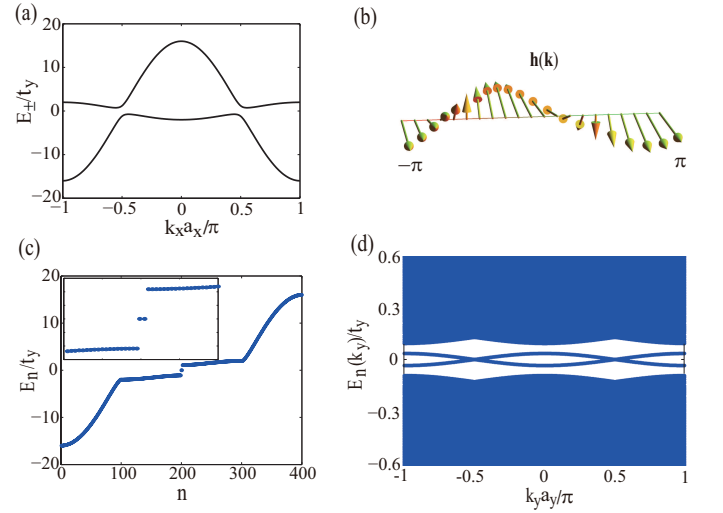

FIG. 2: (a) The single-particle band structure calculated from the tight binding model (Eq. (2)) in quasi-1D limit, when $t_x/t_y = 8$, $t/t_y = 0.6$. (b) Topological winding of Hamiltonian in Eq. (3) across the Brillouin zone. (c) Energy spectrum of the Hamiltonian (Eq. (2)) in quasi-1D limit with finite length (lattice sites $N = 200$), when $t_x/t_y = 8$ and $t/t_y = 0.9$. There are two zero-energy states inside the gap which are located at the two outer edges of the system respectively. Here n labels the energy level. (d) The effect of the small transverse tunneling. The midgap bands show a finite curvature along the y direction with open (and periodic) boundary conditions in the x (y) directions when $t_x/t_y = 8$, $t/t_y = 0.1$, $t'_y/t_y = 0.02$ and $t'_x/t'_y = 0.1$.

The essential physics of band mixing is captured by the following multi-orbital tight binding model without considering the full band structure theory,

$$
\begin{aligned}
H_0 =\ & t_x \sum_{\mathbf{r}} C_{p_x}^{\dagger}(\mathbf{r}) C_{p_x}(\mathbf{r} + \vec{e}_x) - t_y \sum_{\mathbf{r}} C_{p_y}^{\dagger}(\mathbf{r}) C_{p_y}(\mathbf{r} + \vec{e}_x) \\
& + t \sum_{\mathbf{r}} C_{p_x}^{\dagger}(\mathbf{r}) C_{p_y}(\mathbf{r} + \vec{e}_x) - t \sum_{\mathbf{r}} C_{p_y}^{\dagger}(\mathbf{r}) C_{p_x}(\mathbf{r} + \vec{e}_x) \\
& - t'_x \sum_{\mathbf{r}} C_{p_x}^{\dagger}(\mathbf{r}) C_{p_x}(\mathbf{r} + \vec{e}_y) + t'_y \sum_{\mathbf{r}} C_{p_y}^{\dagger}(\mathbf{r}) C_{p_y}(\mathbf{r} + \vec{e}_y) \\
& + h.c. - \mu \sum_{\mathbf{r}} [C_{p_x}^{\dagger}(\mathbf{r}) C_{p_x}(\mathbf{r}) + C_{p_y}^{\dagger}(\mathbf{r}) C_{p_y}(\mathbf{r})], \quad (2)
\end{aligned}
$$

where $C_{\nu}(\mathbf{r})$ is a fermionic annihilation operator for the localized ν orbital (p_x or p_y) located at the lattice site $\mathbf{r}$ and the chemical potential is denoted by μ. The tunnelings (t'_x, t'_y) in the y direction are much weaker compared to that (t_x, t_y) along the x direction, due to the relatively stronger confinement in the y direction. The relative sign of the hopping amplitude is fixed by the parity of p_x and p_y orbitals. The key ingredient in our model is the hybridization between p_x and p_y orbitals. It arises from the asymmetric shape of the p_y orbital wavefunction induced by the inversion symmetry breaking in the y direction. This asymmetry leads to the orbital hybridization $t \sum_{\mathbf{r}} [C_{p_x}^{\dagger}(\mathbf{r}) C_{p_y}(\mathbf{r} + \vec{e}_x) - C_{p_y}^{\dagger}(\mathbf{r}) C_{p_x}(\mathbf{r} + \vec{e}_x)] + h.c.$ in Eq. (2), which plays a crucial

role in producing topological non-trivial band structures. It resembles spin-orbit coupling [47–49] when the p_x and p_y orbitals are mapped to pseudo-spin-1/2 states. But unlike the spin-orbit coupling, the orbital hybridization is geometrically controllable through manipulating the inversion symmetry of the optical lattice.

III. ORBITAL HYBRIDIZED TOPOLOGICAL BAND STRUCTURES

We first focus on the quasi-one dimensional limit where the transverse (y direction) tunnelings are negligible. At half filling (one particle per lattice site), in the basis of $(C^\dagger_{p_x}(\mathbf{k}), C^\dagger_{p_y}(\mathbf{k}))$, the Hamiltonian takes a suggestive form

$$H_0(\mathbf{k}) = h_0(\mathbf{k})\mathbb{I} + \mathbf{h}(\mathbf{k}) \cdot \sigma, \qquad (3)$$

where $h_0(\mathbf{k}) = (t_x - t_y)\cos(k_x a_x)$, $h_x(\mathbf{k}) = 0$, $h_y(\mathbf{k}) = -2t\sin(k_x a_x)$, $h_z(\mathbf{k}) = (t_x + t_y)\cos(k_x a_x)$, and $\sigma_{x,y,z}$ are Pauli matrices. The energy spectrum reads $E_\pm = h_0(\mathbf{k}) \pm \sqrt{h_y^2(\mathbf{k}) + h_z^2(\mathbf{k})}$. As shown in Fig. 2(a), the system is in an insulating state with a band gap determined by the orbital hybridization t. It is a Z_2 topological insulator protected by time reversal and reflection symmetries [50]. Here, the reflection symmetry breaking is along the direction (y-direction) perpendicular to the dynamical direction (x-direction). In sharp contrast to the previous studies [51, 52], the inversion symmetry of the 1D system here is still preserved. To visualize the topological properties of the band structures, we show the vector $\mathbf{h}(\mathbf{k})$ winds an angle of 2π when the momentum $\mathbf{k}$ varies from $-\pi$ to π crossing the entire Brillouin zone (BZ) in Fig. 2(b). It is also confirmed from the calculation of winding number defined as $W = \oint \frac{dk_x}{4\pi}\epsilon_{\eta\eta'}\hat{h}_\eta^{-1}(k_x)\partial_{k_x}\hat{h}_\eta$ with $\hat{h} \equiv \frac{\mathbf{h}}{|\mathbf{h}|}$ and $\epsilon_{yz} = -\epsilon_{zy} = 1$. When $t \neq 0$, the winding number is 1, which signifies a topological band insulator state. The non-trivial topology of this state also manifests through the existence of the edge states. As shown in Fig. 2(c), there are two emergent zero-energy modes located at the two outer edges of the system respectively.

Next we will discuss the effect of the small transverse (y direction) tunneling, which has been neglected above but always exists in a realistic quasi-one dimensional system. By considering small transverse tunneling, the zero-energy modes of individual chain will morph into a midgap band, with finite curvature in the transverse direction as shown in Fig. 2(d). The topological band insulator state remains stable at small value of transverse tunneling. For example, when $t_x/t_y = 8$ and $t/t_y = 0.1$, the topological state survives until t'_y/t_y reaches 0.073 with $t'_x = 0.1t'_y$. However, beyond this value, the band gap will close and the topological band insulator state becomes unstable.
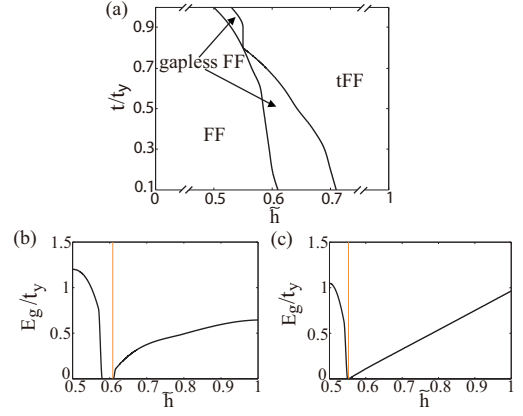

FIG. 3: (a) Zero-temperature phase diagram as a function of the polarization $\tilde{h}$ and orbital hybridization t with fixed $\tilde{\mu}$. Other parameters are $t_x/t_y = 8$, $t'_y/t_y = 0.05$, $t'_x/t'_y = 0.1$, $U/t_y = -15$, $\tilde{\mu} = 0.4$, and $\Omega_z/t_y = 0.3$. (b) and (c) The quasi-particle exaction gap E_g as a function of polarization $\tilde{h}$ when $t/t_y = 0.6$ and $t/t_y = 0.8$ respectively. The vertical lines mark the point where the Z_2 topological invariant changes.

IV. TOPOLOGICAL FULDE-FERRELL STATE AND MAJORANA FERMIONS

In this section, we study attractive fermions in the topological noncentrosymmetric optical lattice (Eq. (1)) with onsite rotation [33] and show that a topological Fulde-Ferrell superfluid state (tFF) with finite center-of-mass momentum emerges. The interacting model to describe this fermionic system is

$$H = H_0 + H_{int} + H_L + H_Z. \qquad (4)$$

In this model, the interaction $H_{int} = U\sum_{\mathbf{r}} C^\dagger_{p_x}(\mathbf{r})C_{p_x}(\mathbf{r})C^\dagger_{p_y}(\mathbf{r})C_{p_y}(\mathbf{r})$ can be induced by considering optical Feshbach resonance [53, 54], Bose-Fermi mixtures [55] or dipolar atoms/molecules [56]. $H_L = i\Omega_z \sum_{\mathbf{r}}[C^\dagger_{p_x}(\mathbf{r})C_{p_y}(\mathbf{r}) - C^\dagger_{p_y}(\mathbf{r})C_{p_x}(\mathbf{r})]$ is the orbital Zeeman energy induced by onsite rotation. Here we assume that the energy of the orbital Zeeman term is much smaller than the band gap. Therefore, its effect is considered within the p_x and p_y orbitals only. The onsite rotation experiment has been achieved in a triangular optical lattice [33], and the techniques are expected applicable to other lattices as well. Through a combination of electro-optic phase modulators of the laser beams forming the lattice and the modulations of potential depth, we propose a method to realize the onsite rotation in the noncentrosymmetric optical lattice (Eq. (1)) (see details in Appendix C). H_Z is the orbital splitting $h\sum_{\mathbf{r}}[C^\dagger_{p_x}(\mathbf{r})C_{p_x}(\mathbf{r}) - C^\dagger_{p_y}(\mathbf{r})C_{p_y}(\mathbf{r})]$. Through adjusting the lattice depth or lattice spacing in the x and y directions, the potential parameters can be tuned to be $V_X k_{Lx}^2 = \alpha V_Y k_{Ly}^2$. With $\alpha \neq 1$, a finite orbital Zeeman splitting H_Z between p_x and p_y orbitals is obtained. In the presence of onsite rotation, i.e., $\Omega_z \neq 0$, both time-reversal and reflection symmetries of the system are broken, and the Fermi surface of the system

becomes asymmetric along the x direction. The pairing with the center-of-mass momentum $\mathbf{Q}$ and $-\mathbf{Q}$ are no longer degenerate. The Fulde-Ferrell (FF) state with a plane wave order parameter $\propto e^{i\mathbf{Q}\cdot\mathbf{r}}$ is more energetically favorable as compared to the Larkin-Ovchinnikov state with a stripe order $\propto \cos(\mathbf{Q}\cdot\mathbf{r})$. This mechanism is crucially different from the system with Raman-induced spin-orbit coupling, where both combined spin-space rotation and mirror symmetries need to be broken [34–42].

Taking the superfluid pairing order parameter $\Delta(\mathbf{r}) = U\langle C_{p_y}(\mathbf{r})C_{p_x}(\mathbf{r})\rangle = \Delta e^{i\mathbf{Q}\cdot\mathbf{r}}$, the system is described by the Bogoliubov-de-Gennes (BdG) Hamiltonian at mean field level. Since the weak transverse hopping introduces a small Fermi surface curvature, we expect the center-of-mass momentum of pairing $\mathbf{Q}$ pointing along the x direction, say $\mathbf{Q} = Q(1,0)$, in order to maximize the phase space of pairing. Through diagonalizing the BdG Hamiltonian, we obtain the free energy of the system. The pairing order parameter Δ and the center-of-mass momentum of pairing $\mathbf{Q}$ are determined from minimizing the free energy. The details are given in the Appendix A. We find that when $\Omega_z > 0$ the center-of-mass momentum of pairing along the x direction is selected as a certain positive Q due to the deformation of the Fermi surface. Since the p_x and p_y bands have different bandwidths, we introduce two dimensionless quantities $\tilde{\mu}_{p_x} = \frac{\mu-h}{2t_x}$ and $\tilde{\mu}_{p_y} = \frac{\mu+h}{2t_y}$, which respectively control the average filling of the two p bands. Correspondingly, we also introduce a dimensionless chemical potential $\tilde{\mu} = \frac{\tilde{\mu}_{p_x}+\tilde{\mu}_{p_y}}{2}$ and orbital polarization $\tilde{h} = \frac{\tilde{\mu}_{p_y}-\tilde{\mu}_{p_x}}{2}$. For fixed $\tilde{\mu}$, the resulting phase diagram as a function of $\tilde{h}$ and the orbital hybridization t is shown in Fig. 3(a). There are two first order phase transitions as the polarization $\tilde{h}$ is increased (except at $t/t_y \approx 0.8$). The first one is a transition from a gapped FF superfluid to a gapless FF superfluid state (with Bogoliubov quasi-particles being gapless). The gap closing across the phase transition is shown in Fig. 3(b). Further increasing the polarization, the second one occurs between the gapless FF and tFF superfluid states. When $t/t_y \approx 0.8$, there is only one phase transition from FF to tFF superfluid states without passing through the gapless FF superfluids, since we find in Fig. 3(c) that E_g will firstly close and reopen immediately. We also find that a finite polarization is required to stabilize the tFF superfluid state. The critical polarization $\tilde{h}_c$ decreases as the orbital hybridization t increases.

The transition from non-topological to topological FF states here can be understood by observing the non-trivial Z_2 topological invariant. The BdG Hamiltonian (See details in Appendix A) maintains the particle-hole symmetry, i.e.,

$$\Xi H_{BdG}(\mathbf{k})\Xi^{-1} = -H_{BdG}^*(-\mathbf{k}), \text{ with } \Xi = \begin{pmatrix} 0 & \mathbb{I} \\ \mathbb{I} & 0 \end{pmatrix},$$ while

the time reversal and chiral symmetries are broken. Therefore, the tFF superfluid state predicted here belongs to the D symmetry class according to the general classification scheme of topological superconductors [50]. This topological state is thus characterized by a Z_2 topological invariant [57, 58]. As shown in Fig. 3(b) and (c), we find that the Z_2 topological invariant (see Appendix B for explanation) $M = -1$ in the
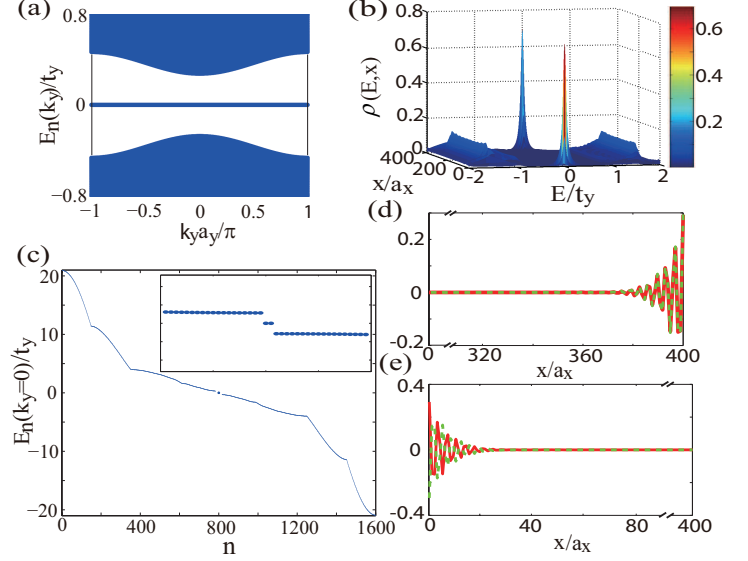

FIG. 4: (a) Energy spectrum of the Hamiltonian in Eq. (4) under the mean-field approximation with open (and periodic) boundary conditions in the x (y) directions. There is a doubly degenerate flat band composed of Majorana fermions when the transverse tunneling is small. (b) The local density of states (LDOS) (see the main text). The zero-energy peaks of the LDOS are located at the two edges of the system respectively. (c) Energy spectra with $k_y a_y = 0$. There are two degenerate zero energy states. (d) and (e), The wavefunctions of the two Majorana zero-energy modes as shown in (c), which satisfy $u_{0,p_x} = v_{0,p_x}^*$ at the right edge and $u_{0,p_x} = -v_{0,p_x}^*$ at the left edge (other components of these two wavefunctions, say u_{0,p_y} and v_{0,p_y}, also satisfy the same relations). These two states support two local Majorana fermions at two outer edges of the system respectively. Here we choose finite length along the x direction with lattice sites $N = 400$ and $\tilde{h} = 0.7$, $t/t_y = 0.6$. Other parameters are the same as in Fig. 3 and n denotes the energy level.

tFF superfluid state and $M = 1$ in the gapless FF superfluid state. This gapless state is topologically trivial (see Appendix D for details), which is different from the state found in the previous studies [40–42].

To further demonstrate the topological nature of the tFF superfluid phase, we will show Majorana fermions are supported in this state. To see this, we consider a cylinder geometry of the system, where the open (periodic) boundary condition is chosen in the $x(y)$ direction respectively. The energy spectrum in Fig. 4(a) is labeled by the momentum k_y. As shown in Fig. 4(a), all the bulk modes are gapped and there are two degenerate flat bands composed of Majorana fermions located at the two outer edges of the system respectively. As shown in Fig. 4(c), for a fixed k_y, there are two zero-energy states located at the two outer edges of the system. The corresponding wavefunctions $(u_{0,\nu}, v_{0,\nu})^T$ satisfy the relation $u_{0,\nu}(x) = v_{0,\nu}^*(x)$ $[u_{0,\nu}(x) = -v_{0,\nu}^*(x)]$ on the right [left] edge (Fig. 4(d) and (e)). These eigenstates support localized Majorana fermions at the edges of the system. These Majorana fermions are signified through the local density of states (LDOS) which can be measured by radio-frequency (rf)

spectroscopy [59–61]. The LDOS is calculated as $\rho(x,E) = (1/2)\sum_{n,\nu}\int dk_y[|u_{n,\nu}|^2\delta(E-\zeta_n) + |v_{n,\nu}|^2\delta(E+\zeta_n)]$, where $(u_{n,\nu}, v_{n,\nu})^T$ is the eigenvector corresponding to the eigenenergy ζ_n of the mean-field BdG Hamiltonian with cylinder geometry. We find that the zero-energy Majorana fermions manifest themselves by a peak in LDOS located at the edges of the system, as shown in Fig. 4(b). This spatially localized zero-energy peak in LDOS can be detected using spatially resolved radio-frequency (rf) spectroscopy technique [61], which would provide a concrete signature for the experiment. We also study the effect of small transverse tunneling on the stability of tFF superfluids (see details in Appendix E).

V. CONCLUSION

We have developed a systematic approach to the control of non-trivial orbital hybridization in a static noncentrosymmetric optical lattice, which is shown to exhibit unconventional topological properties. This approach is rather generic to optical lattices than restricted to the setup considered in this work. Its principle is readily generalizable to higher dimensions with straightforward modifications, potentially circumventing the challenges in Raman-induced

spin-orbit coupling scheme [47–49, 62, 63]. Moreover, our proposal is still within the static system instead of an inherently time-dependent Hamiltonian problem, e.g., shaking optical lattices [16, 64], whose understanding is still quite open. The present approach thus complements with a new window to investigate topological phases in cold gases.

Appendix A: BdG equation in momentum space

Through introducing the superfluid pairing order parameter $\Delta(\mathbf{r}) = U\langle C_{p_y}(\mathbf{r})C_{p_x}(\mathbf{r})\rangle = \Delta e^{i\mathbf{Q}\cdot\mathbf{r}}$, the system can be described by the Bogoliubov-de-Gennes (BdG) Hamiltonian at mean-field level

$$H_{BdG}(\mathbf{k}) = \begin{pmatrix} \varepsilon_{p_x}(\mathbf{Q/2}+\mathbf{k}) & \varepsilon(\mathbf{Q/2}+\mathbf{k}) & 0 & \Delta \\ -\varepsilon(\mathbf{Q/2}+\mathbf{k}) & \varepsilon_{p_y}(\mathbf{Q/2}+\mathbf{k}) & -\Delta & 0 \\ 0 & -\Delta^* & -\varepsilon_{p_x}(\mathbf{Q/2}-\mathbf{k}) & \varepsilon(\mathbf{Q/2}-\mathbf{k}) \\ \Delta^* & 0 & -\varepsilon(\mathbf{Q/2}-\mathbf{k}) & -\varepsilon_{p_y}(\mathbf{Q/2}-\mathbf{k}) \end{pmatrix}, \tag{A1}$$

where the Nambu basis is chosen to be $(C_{p_x}(\mathbf{Q/2}+\mathbf{k}), C_{p_y}(\mathbf{Q/2}+\mathbf{k}), C_{p_x}^\dagger(\mathbf{Q/2}-\mathbf{k}), C_{p_y}^\dagger(\mathbf{Q/2}-\mathbf{k}))^T$, $\varepsilon_{p_x}(\mathbf{k}) = 2t_x\cos(k_xa_x) - 2t'_x\cos(k_ya_y) - (\mu - h)$, $\varepsilon_{p_y}(\mathbf{k}) = -2t_y\cos(k_xa_x) + 2t'_y\cos(k_ya_y) - (\mu + h)$ and $\varepsilon(\mathbf{k}) = 2it\sin(k_xa_x) + i\Omega_z$.

Then, the free energy can be obtained by diagonalizing the BdG Hamiltonian in Eq. (A1) by standard procedure as

$$F[\Delta] = 1/2\sum_{\mathbf{k}}[\varepsilon_{p_x}(\mathbf{k}) + \varepsilon_{p_y}(\mathbf{k}) \\ + \sum_\lambda \Theta(-E_\lambda(\mathbf{k}))E_\lambda(\mathbf{k})] - \frac{N|\Delta|^2}{U},$$

where E_λ is the quasi-particle energy, and Θ is the Heaviside step function. The pairing order parameter Δ and the center-of-mass momentum of pairing $\mathbf{Q}$ can be determined from minimizing the free energy.

Appendix B: Z_2 topological invariant

To characterize the topological nature of the tFF superfluid state, we calculate the Z_2 topological invariant. Here, we introduce the Majorana operators as $\gamma^A(\mathbf{r}) = C_{p_x}^\dagger(\mathbf{r}) + C_{p_x}(\mathbf{r})$, $\gamma^B(\mathbf{r}) = [C_{p_x}(\mathbf{r}) - C_{p_x}^\dagger(\mathbf{r})]/i$, $\gamma^C(\mathbf{r}) = C_{p_y}^\dagger(\mathbf{r}) + C_{p_y}(\mathbf{r})$ and $\gamma^D(\mathbf{r}) = [C_{p_y}(\mathbf{r}) - C_{p_y}^\dagger(\mathbf{r})]/i$, which fulfill the relations $\gamma^{\dagger\alpha}(\mathbf{r}) = \gamma^\alpha(\mathbf{r})$ and the anticommutation relations $\{\gamma^\alpha, \gamma^\beta\} = 2\delta_{\alpha\beta}\delta(\mathbf{r}-\mathbf{r}')$ with α or β taking A, B, C or D. In terms of Majorana operators, the Hamiltonian in Eq. (4) under the mean-field approximation can be represented as $H_{MF} = \frac{i}{4}\sum_{l,m=1}^{4N}A_{lm}\gamma_l\gamma_m$ with $\gamma_{4j-3} = \gamma^A(\mathbf{r}_j)$, $\gamma_{4j-2} = \gamma^B(\mathbf{r}_j)$, $\gamma_{4j-1} = \gamma^C(\mathbf{r}_j)$ and $\gamma_{4j} = \gamma^D(\mathbf{r}_j)$, where j runs over all the N lattice sites and A is a skew-symmetric matrix. The Pfaffian of matrix A is defined as $\text{Pf}(A) = \frac{1}{2^n n!}\sum_{\tau\in S_{2n}}sgn(\tau)\prod_{m=1}^n A_{\tau(2m-1),\tau(2m)}$ with $n = 2N$, where S_{2n} is the set of permutation and $sgn(\tau)$ is the corresponding sign of that. The Z_2 topological invariant is defined as $M = sgn[\text{Pf}(A)]$ when choosing the periodic boundary condition. The Z_2 topological non-trivial phase is characterized by $M = -1$, where as the topological trivial
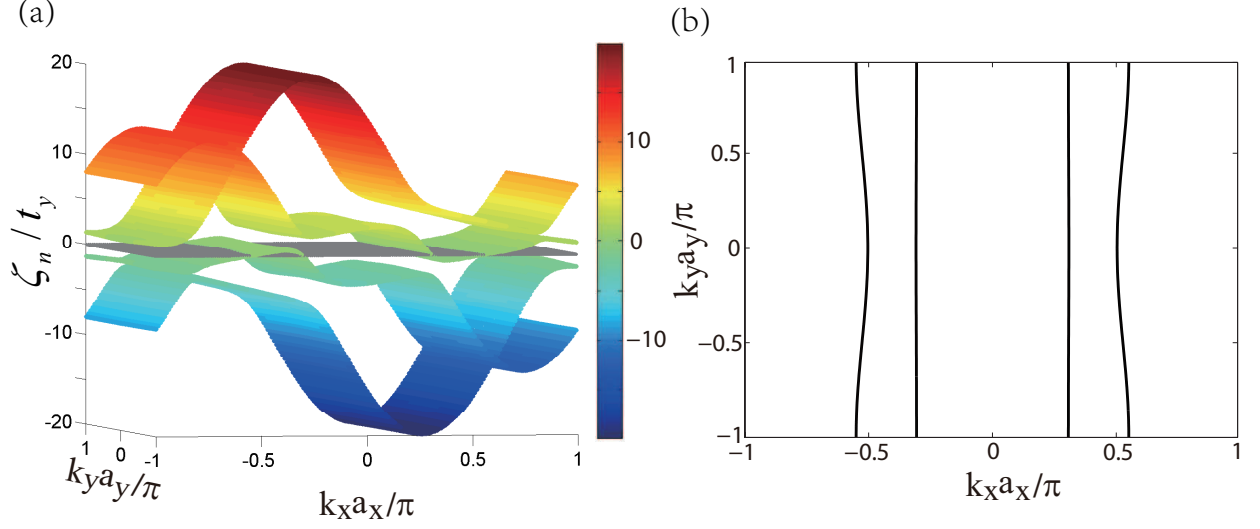
FIG. A1: (a) Quasiparticle excitations of the gapless topological FF superfluids in the (k_x, k_y) plane , where $\tilde{h} = 0.62$, $t/t_y = 0.5$ and other parameters are the same as in Fig. 3(a). The grey color plane corresponds to zero excitation energy. (b) The contours of zero-energy excitations (nodal points).

phase corresponds to $M = 1$.

Appendix C: Onsite rotation in noncentrosymmetric optical lattices

Through putting electro-optic modulators on the laser beams forming the lattice [65] and also employing modulations of potential depth [66], the lattice potential can be expressed as

$$
\begin{aligned}
V'(x,y) &= \frac{1}{2}\sum_{\gamma=\pm}[-V_X\cos^2(k_{Lx}x+\phi_\gamma) - V_Y\cos^2(k_{Ly}y+\phi_\gamma) + V_{\bar{Y}}\cos^2(3k_{Ly}y+\pi/4+\phi_\gamma)] \\
&- \delta V_X\cos^2(k_{Lx}x+\pi/4) - \delta V_Y\cos^2(k_{Ly}y+\tilde{\phi}),
\end{aligned}
\tag{C1}
$$

where the electro-optic phase modulators $\phi_+ = \Delta\phi\cos(\Omega_z t)\cos(\omega_{RF}t)$, $\phi_- = \Delta\phi\sin(\Omega_z t)\cos(\omega_{RF}t)$ with the slow precession frequency Ω_z, the amplitude of oscillation $\Delta\phi$ and the fast rotation frequency ω_{RF} at radio frequency. $\delta V_X = \tilde{V}_X\sin(\Omega_z t)$ and $\delta V_Y = \tilde{V}_Y\cos(\Omega_z t)$ are the modulation amplitudes of the lattice depth and $\tilde{\phi}$ is a certain phase. It results in a periodical overall translation of the lattice at a radio-frequency ω_{RF}. Atoms do not follow the fast oscillation at radio frequency ω_{RF} and only feel a time averaged potential. The local potential near each site minimum in the rotating frame with frequency Ω_z is then approximately (dropping a constant) $V'_{eff}(\mathbf{r}') \simeq \frac{1}{2}m\omega_0^2(1 - \frac{(\Delta\phi)^2}{2})r'^2 + \tilde{V}_X k_{Lx}y'$ with ω_0 the radial vibration frequency of a lattice site without modulation, when considering $V_X k_{Lx}^2 = \beta V_Y k_{Ly}^2$, $\beta = \cos(2k_{Ly}y_0) + 9\sin(6k_{Ly}y_0)$, $\tilde{V}_X k_{Lx} = \tilde{V}_Y k_{Ly}$ and $\tan(2\tilde{\phi}) = \cot(2k_{Ly}y_0)$, where y_0 is determined by $\cos(6k_{Ly}y_0)/\sin(2k_{Ly}y_0) = V_Y/3V_{\bar{Y}}$. Therefore, each lattice site rotates around its own center with frequency Ω_z, meanwhile keeping the reflection symmetry breaking along the y-direction. The onsite rotation technique is thus adopted to our noncentrosymmetric optical lattices.

Appendix D: Gapless Fulde-Ferrell state

Since the p_x and p_y bands are highly anisotropically dispersive, the Fermi surface are the slightly curved lines across the entire Brillouin zone. As a result, the nodal points

of the excitation in our predicted gapless Fulde-Ferrell state will not form two disjoint loops in the momentum space (Fig. A1). It is essentially different from the state found in the previous studies of the system with Raman-induced spin-orbit coupling. Furthermore, this gapless state is a topologically trivial state, having a trivial Z_2 topological invariant $M = 1$.

Appendix E: Stability of tFF superfluids

Here, We discuss the effect of small transverse tunneling on the stability of tFF superfluids. The transverse hopping term restores the 2D nature of the Fermi surface, which acquires a finite curvature in the transverse direction. It suppresses the perfect nesting, therefore it disfavors the tFF superfluid state. Our numerical result indicates that the tFF superfluity remains stable at small value of transverse tunneling. For example, the tFF superfluid state, as shown in Fig. 3(a) with $t/t_y = 0.8$ and $\tilde{h} = 0.7$, survives until t'_y/t_y reaches 0.2 and the flat bands composed of Majorana fermions in a cylinder geometry will be maintained [67]. Beyond this value, the bulk gap will close and the tFF superfluids become unstable.

[1] K. V. Samokhin, Ann. Phys. **324**, 2385 (2009).
[2] S. Mühlbauer, B. Binz, F. Jonietz, C. Pfleiderer, A. Rosch, A. Neubauer, R. Georgii, and P. Böni, Science **323**, 915 (2009).
[3] X. Z. Yu, Y. Onose, N. Kanazawa, J. H. Park, J. H. Han, Y. Matsui, N. Nagaosa, and Y. Tokura, Nature **465**, 901 (2010).
[4] S. Seki, X. Z. Yu, S. Ishiwata, and Y. Tokura, Science **336**, 198 (2012).
[5] K. V. Samokhin, Phys. Rev. B **70**, 104521 (2004).
[6] V. P. Mineev and K. V. Samokhin, Phys. Rev. B **78**, 144503 (2008).
[7] A. P. Schnyder and S. Ryu, Phys. Rev. B **84**, 060504 (2011).
[8] P. M. R. Brydon, A. P. Schnyder, and C. Timm, Phys. Rev. B **84**, 020501 (2011).
[9] S. Fujimoto, Phys. Rev. B **72**, 024515 (2005).
[10] S. K. Yip, Phys. Rev. B **65**, 144508 (2002).
[11] L. Tarruell, D. Greif, T. Uehlinger, G. Jotzu, and T. Esslinger, Nature **483**, 302 (2012).
[12] R. Wang, C.-X. Zhang, and Q.-S. Ji, Chin. Phys. B **24**, 30305 (2015).
[13] T. Müller, S. Fölling, A. Widera, and I. Bloch, Phys. Rev. Lett. **99**, 200405 (2007).
[14] G. Wirth, M. Ölschläger, and A. Hemmerich, Nat. Phys. **7**, 147 (2011).
[15] P. Soltan-Panahi, D.-S. Lühmann, J. Struck, P. Windpassinger, and K. Sengstock, Nat. Phys. **8**, 71 (2012).
[16] C. V. Parker, L.-C. Ha, and C. Chin, Nat. Phys. **9**, 769 (2013).
[17] T. Kock, M. Ölschläger, A. Ewerbeck, W.-M. Huang, L. Mathey, and A. Hemmerich, Phys. Rev. Lett. **114**, 115301 (2015).
[18] For a perspective and brief review, see, for example, M. Lewenstein, and W. V. Liu, Nat. Phys. **7**, 101 (2011).
[19] K. Sun, W. V. Liu, A. Hemmerich, and S. Das Sarma, Nat. Phys. **8**, 67 (2012).
[20] X. Li, E. Zhao, and W. V. Liu, Nat. Commun. **4**, 1523 (2013).
[21] B. Liu, X. Li, B. Wu, and W. V. Liu, Nat. Commun. **5**, 5064 (2014).
[22] C. Wu, Phys. Rev. Lett. **100**, 200406 (2008).
[23] C. Wu, Phys. Rev. Lett. **101**, 186807 (2008).
[24] S.-L. Zhang and Q. Zhou, Phys. Rev. A **90**, 051601 (2014).
[25] W. Zheng and H. Zhai, Phys. Rev. A **89**, 061603 (2014).
[26] S. K. Baur, M. H. Schleier-Smith, and N. R. Cooper, Phys. Rev. A **89**, 051605 (2014).
[27] V. Galitski and I. B. Spielman, Nature **494**, 49 (2013).
[28] H. Zhai, Int. J. Mod. Phys. B **26**, 1230001 (2012).
[29] R. A. Hart, P. M. Duarte, T.-L. Yang, X. Liu, T. Paiva, E. Khatami, R. T. Scalettar, N. Trivedi, D. A. Huse, and R. G. Hulet, Nature **519**, 211 (2015).
[30] Y.-a. Liao, A. S. C. Rittner, T. Paprotta, W. Li, G. B. Partridge, R. G. Hulet, S. K. Baur, and E. J. Mueller, Nature **467**, 567 (2010).
[31] G. B. Partridge, W. Li, R. I. Kamar, Y.-a. Liao, and R. G. Hulet, Science **311**, 503 (2006).
[32] M. W. Zwierlein, A. Schirotzek, C. H. Schunck, and W. Ketterle, Science **311**, 492 (2006).
[33] N. Gemelke, E. Sarajlic, and S. Chu, arXiv **:1007.2677** (2010).
[34] W. Zhang and W. Yi, Nat. Commun. **4**, 2711 (2013).
[35] C. Qu, Z. Zheng, M. Gong, Y. Xu, L. Mao, X. Zou, G. Guo, and C. Zhang, Nat. Commun. **4**, 2710 (2013).
[36] C. Chen, Phys. Rev. Lett. **111**, 235302 (2013).
[37] X.-J. Liu and H. Hu, Phys. Rev. A **88**, 023622 (2013).
[38] C. F. Chan and M. Gong, Phys. Rev. B **89**, 174501 (2014).
[39] L. Jiang, E. Tiesinga, X.-J. Liu, H. Hu, and H. Pu, Phys. Rev. A **90**, 053606 (2014).
[40] Y. Xu, R.-L. Chu, and C. Zhang, Phys. Rev. Lett. **112**, 136402 (2014).
[41] Y. Cao, S.-H. Zou, X.-J. Liu, S. Yi, G.-L. Long, and H. Hu, Phys. Rev. Lett. **113**, 115302 (2014).
[42] H. Hu, L. Dong, Y. Cao, H. Pu, and X.-J. Liu, Phys. Rev. A **90**, 033624 (2014).
[43] X.-J. Liu, H. Hu, and H. Pu, Chin. Phys. B **24**, 50502 (2015).
[44] G. G. Batrouni, M. J. Wolak, F. Hébert, and V. G. Rousseau, Europhys. Lett. **86**, 47006 (2009).
[45] X. Li, Z. Zhang, and W. V. Liu, Phys. Rev. Lett. **108**, 175302 (2012).
[46] E. Zhao and W. V. Liu, Phys. Rev. Lett. **100**, 160403 (2008).
[47] Y.-J. Lin, K. Jiménez-García, and I. B. Spielman, Nature **471**, 83 (2011).
[48] L. W. Cheuk, A. T. Sommer, Z. Hadzibabic, T. Yefsah, W. S. Bakr, and M. W. Zwierlein, Phys. Rev. Lett. **109**, 095302 (2012).
[49] P. Wang, Z.-Q. Yu, Z. Fu, J. Miao, L. Huang, S. Chai, H. Zhai, and J. Zhang, Phys. Rev. Lett. **109**, 095301 (2012).
[50] A. P. Schnyder, S. Ryu, A. Furusaki, and A. W. W. Ludwig, Phys. Rev. B **78**, 195125 (2008).
[51] B.-J. Yang, M. S. Bahramy, R. Arita, H. Isobe, E.-G. Moon, and N. Nagaosa, Phys. Rev. Lett. **110**, 086402 (2013).
[52] J. Liu and D. Vanderbilt, Phys. Rev. B **90**, 155316 (2014).
[53] R. Yamazaki, S. Taie, S. Sugawa, K. Enomoto, and Y. Takahashi, Phys. Rev. A **87**, 010704 (2013).
[54] K. Goyal, I. Reichenbach, and I. Deutsch, Phys. Rev. A **82**, 062704 (2010).
[55] M. J. Bijlsma, B. A. Heringa, and H. T. C. Stoof, Phys. Rev. A

61, 053601 (2000).

[56] M. A. Baranov, M. Dalmonte, G. Pupillo, and P. Zoller, Chem. Rev. **112**, 5012 (2012).

[57] A. Y. Kitaev, Phys. Usp. **44**, 131 (2001).

[58] P. Ghosh, J. D. Sau, S. Tewari, and S. Das Sarma, Phys. Rev. B **82**, 184525 (2010).

[59] S. Gupta, Z. Hadzibabic, M. W. Zwierlein, C. A. Stan, K. Dieckmann, C. H. Schunck, E. G. M. van Kempen, B. J. Verhaar, and W. Ketterle, Science **300**, 1723 (2003).

[60] C. A. Regal and D. S. Jin, Phys. Rev. Lett. **90**, 230404 (2003).

[61] Y. Shin, C. H. Schunck, A. Schirotzek, and W. Ketterle, Phys. Rev. Lett. **99**, 090403 (2007).

[62] L. Huang, Z. Meng, P. Wang, P. Peng, S.-L. Zhang, L. Chen, D. Li, Q. Zhou, and J. Zhang, arXiv **:1506.02861** (2015).

[63] J. Dalibard, F. Gerbier, G. Juzeliūnas, and P. Öhberg, Rev. Mod. Phys. **83**, 1523 (2011).

[64] M. A. Khamehchi, C. Qu, M. E. Mossman, C. Zhang, and P. Engels, arXiv **:1506.03887** (2015).

[65] N. Gemelke, Ph.D. thesis (2007).

[66] T. Stöferle, H. Moritz, C. Schori, M. Köhl, and T. Esslinger, Phys. Rev. Lett. **92**, 130403 (2004).

[67] C. Qu, M. Gong, Y. Xu, S. Tewari, and C. Zhang, arXiv **:1310.7557** (2013).